Bulletin of the Seismological Society of America, Vol. 93, No. 2, pp. 583–599, April 2003

Identifying 2D Resonance in Microtremor Wave Fields

by Sibylle Steimen, Donat Fäh, Fortunat Kind, Christian Schmid, and Domenico Giardini

Abstract To predict local site effects during earthquakes, we must know the geometrical and mechanical properties of local sedimentary structures and their resonance behavior. We present a concept to identify resonance modes for 2D structures. This is done for synthetic as well as measured microtremor wave fields. The microtremor data were investigated by using the reference station and horizontal-to-vertical (H/V) methods. Analyzing the synthetic microtremor data in profiles across 2D structures, the reference station method (RSM) turned out to be much more suitable for the detection of 2D resonances than the H/V method. We therefore focused on RSM when analyzing the measurement data from two test sites in Switzerland, the St. Jakob–Tüllingen trough near Basel in the north and a site in the Rhone valley near the village Vetroz in the south. The results of these two test sites led to different conclusions. Whereas the spectral peaks in data of the St. Jakob–Tüllingen trough were not well developed and could only tentatively be interpreted, those from the Rhone valley clearly exhibited 2D resonance effects: the SH_{00} and the SV-fundamental mode could be successfully identified at 0.32 ± 0.03 and 0.35 ± 0.03 Hz, respectively.

Introduction

Using the horizontal and vertical spectral ratio of seismic noise, a microzonation study of the Basel area (Fäh *et al.*, 1997), determined the fundamental resonance frequency of the unconsolidated sediments. The St. Jakob–Tüllingen syncline, filled with Tertiary marls, showed a low, constant resonance frequency around 0.4 Hz (Fig. 1A). The authors suggested a 2D resonance due to the syncline shape of this trough. The goal in this study was to investigate a possible 2D effect visible in the microtremor wave field measured over a 2D structure. Using synthetic modeling, we developed a method to identify such 2D resonance effects in the microtremor wave field and tested it at two different measurement sites: the St. Jakob–Tüllingen trough near Basel and the upper Rhone valley near the village of Vetroz (Fig. 1B).

The St. Jakob–Tüllingen syncline is part of the Rhinegraben and bounds this structure to the East (Fig. 1A). The geology of the trough is known, because data from numerous drillholes for groundwater and a few deep wells are available (Hauber, 1991, 1993). The syncline of St. Jakob–Tüllingen has asymmetric geometry, with a steep slope to the East and a gradual slope in the West (Fig. 2B). The structure is filled by Mesozoic deposits (Triassic to Jurassic), covered in turn by Tertiary sediments. The maximum depth to the crystalline rock is about 1700 m; the maximum depth to the first strong impedance contrast, relevant to this study, is about 600 m and lies between the Meletta and the Meeressand layers. The soft sediments consist (from bottom to top) of the Meletta layer (argillaceous marls), the Molasse Alsacienne (sandy marls), and the Tüllinger–Süsswasserschichten (chalks in the northern part of the structure and argillaceous marls more to the South, at the study area).

The subsurface structure of the Rhone valley in the region of Vetroz in Switzerland is well known from a reflection seismic study done there (Pfiffner *et al.*, 1997). The unconsolidated deposits consist of five main layers from bottom to top (Frischknecht et al., 1998): subglacial deposit (gravel), lodgment and till, meltout and reworked till (boulders and fine particles), glaciolacustrine deposit (turbidites, gravel, sand, till), and deltaic sediments. The maximum depth to the sediment rock boundary is 890 m; the width of the structure at the cross section is 3000 m (Fig. 2C).

Because 2D structures tend to amplify ground motion, Bard and Bouchon (1985) analyzed 2D resonance effects in sine-shaped valleys. To calculate frequencies of resonance in such structures, they presented approximate analytical formulas as well as formulas derived from numerical modeling. We could use their results to test and complement our own modeling. We calculated finite difference microtremor spectra along profiles perpendicular to the valley axis of two simplified sine-type structures. Next, we analyzed the synthetic microtremor using the reference station method (RSM) and the horizontal-to-vertical (H/V) spectral ratio. We were able to detect frequencies of resonance corresponding to the values we derived using the Bard and Bouchon (1985) for-

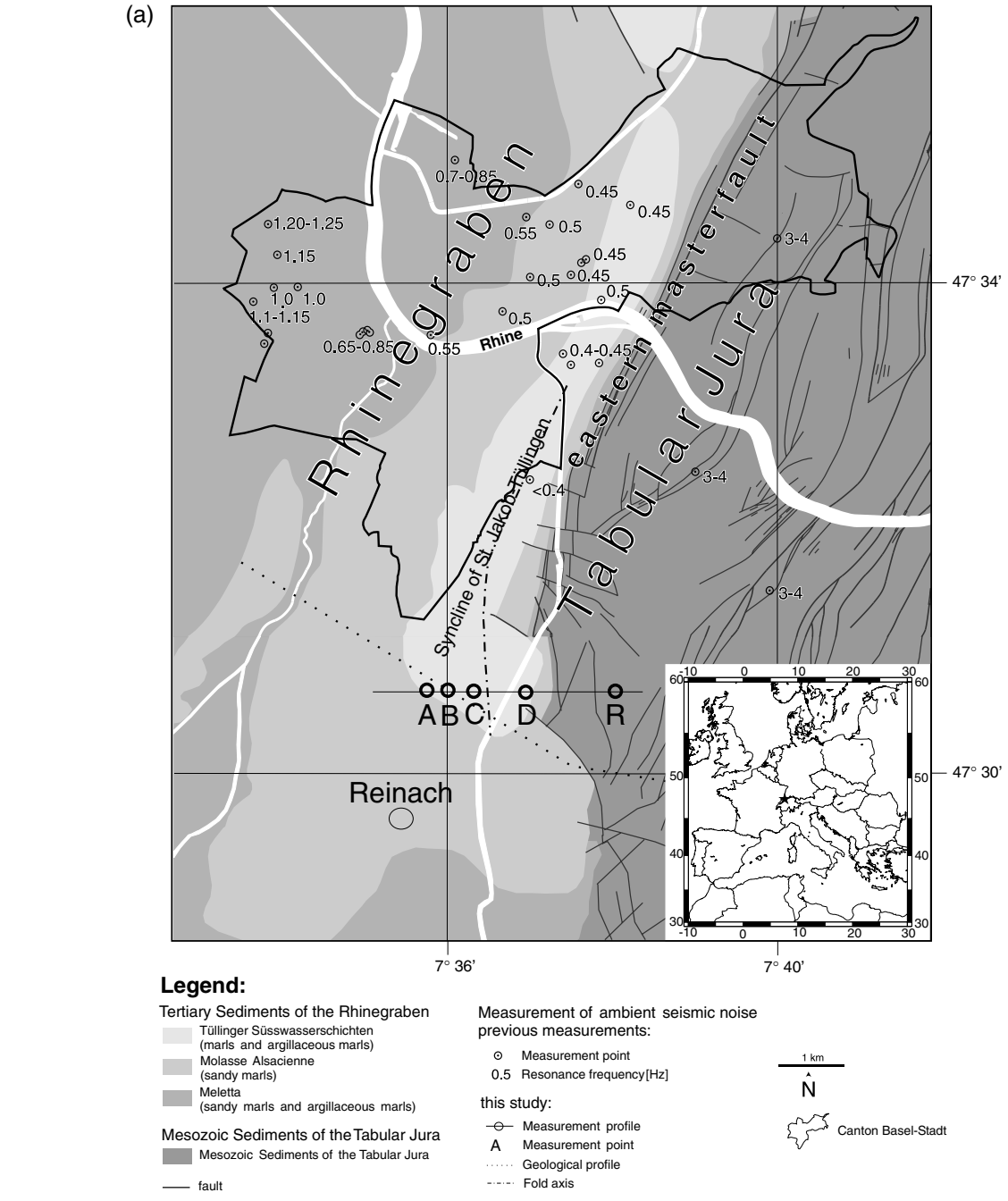

Figure 1. (a) Geographical and geological overview of the study site in Basel, Switzerland. The geological units show the prequaternary surface. The small numbers in the figure give values for resonance frequencies measured using the H/V method by Fäh *et al.* (1997). Major geological units are the Rhinegraben to the west and the Tabular Jura in the east. In between the Syncline of St. Jakob–Tüllingen is marked in light gray. The measurement profile in the southern part of the syncline is marked by a thin black line with the positions of the receivers A to D and the reference R on top of it. The inset gives the location of the measurement site within Europe. (b) Map showing the location of the two measurement sites in Basel and Vetroz within Switzerland.

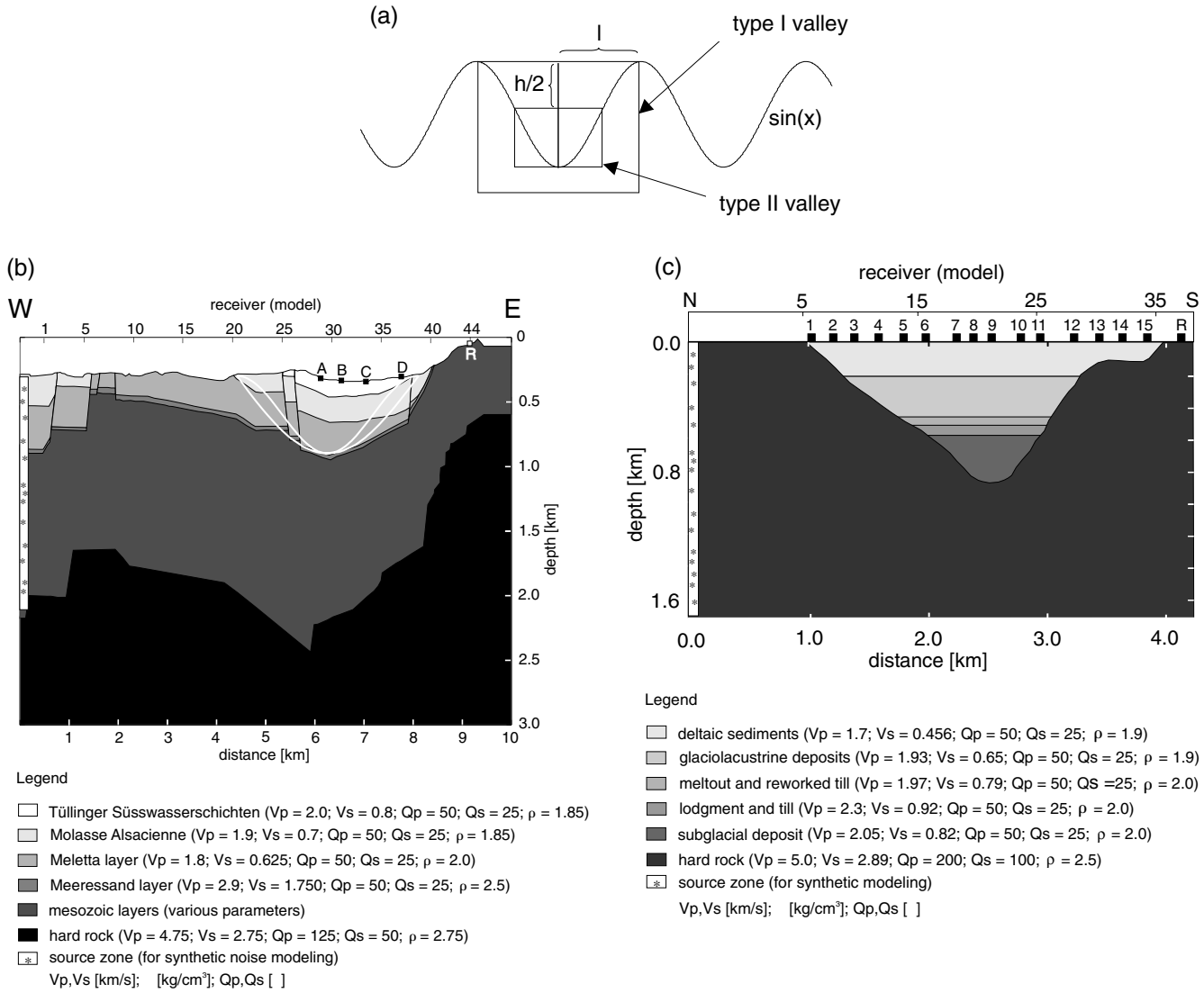

Figure 2. (a) Definition of the sine-type valleys, the two boxes mark the section of the sine curve used for the geometrical shape of the corresponding valley. Both sine-shaped basins have a maximum depth of 0.6 km and a total width of 3.7 km. The trough was supposed to be filled uniformly by Molasse Alsacienne, surrounded by a uniform half-space (V_P = 4.5 km/sec; V_S = 2.4 km/sec; Q_P = 125; Q_S = 50; ρ = 2.3 g/cm^3). (b) Geological cross section through the St. Jakob–Tüllingen trough used as basis for the geometrical model for the complex 2D model of this structure. The white shapes show the geometry of the sine valley approximations within the real model for comparison. The source zone for the modeling process is indicated by the white band with stars to the left of the model; receiver positions in the computation work are given as numbers on the top axis of the figure; receiver positions in the measurement campaign are indicated by letters A to D and R (reference) on the surface of the topmost layer. (c) Geological cross section through the Rhone valley near Vetroz. The cross section shows the model as it was used in the calculation of the synthetic noise with the sources to the left of the model and the receiver positions for the analysis of the synthetic data on the top axis of the figure. Elastic parameters for the sediment layers are given in the legend. The receivers on the topmost layer give the positions of the receivers in the measurement campaign.

mulas. We used this match as evidence that using our modeling and analysis technique would help to detect the resonance frequencies of sediment-filled valleys, at least in those simple structures. We then proceeded to the two realistic structures whose 2D resonance properties we wanted to investigate. After calculating the synthetic microtremor signals, we used the same procedures to analyze the data and then compared the results with those derived from our measured data in Basel and Vetroz.

It should be noted that throughout this article we use the term "microtremor" to address long-period ambient vibrations in the same sense as Ohta *et al.* (1978) used the term "long-period microtremor" for the seismic noise in the period range of 1–5 sec mostly generated by sea waves. In

sections where we use the term "ambient vibrations" or "seismic noise," we speak more generally of ambient vibrations in the whole bandwidth.

2D Resonance in Sediment-Filled Valleys: Basic Concepts

Bard and Bouchon (1985) used the structure of a sine-shaped valley to analyze the effects of the 2D resonance and presented simple analytical formulas as well as formulas derived from numerical computations to estimate the resonance frequencies. Next, we give a short overview of their method. Their starting point was an analytical formula for *SH*-resonance frequencies in a rectangular basin immersed in a homogeneous half-space.

$$f_{mn}^{\mathrm{SH}} = \frac{\beta_1}{4h}\sqrt{(2m+1)^2 + (n+1)^2\frac{h^2}{w^2}}, \qquad (1)$$

where w is the half-width of the basin, h is its depth, β_1 is its seismic *S*-wave velocity, m is the number of nodes in the vertical standing wave, and n the number of nodes in the horizontal. In valley models of arbitrary (nonrectangular) geometry, equation (1) must be adapted using an equivalent width $2w^*$ defined as the length over which the local sediment thickness is greater than half the maximum thickness (Bard and Bouchon, 1985).

For the valley geometries modeled in this study, the equivalent half-width is significantly larger than the depth, and we see from equation (1) that at lower frequency the resonance modes will be those with horizontal nodes (higher order n) rather than those with vertical nodes (higher order m). Following the notation of Bard and Bouchon (1985), the *SH*-harmonics in n are called "symmetric" if they have an amplification maximum at the center of symmetry (even number of n) and "antisymmetrical" (odd number of n) if they have an amplification node at the center of symmetry.

The *PSV* case is more complex because of a coupling of the ground motion of the vertical and the horizontal component. In equations (2) and (3) two laws to calculate the fundamental *SV*- and *P*-resonance frequency are given. They were derived by Bard and Bouchon (1985) from their numerical modeling of resonance modes for a specific valley geometry (in this article referred to as "type I," explained in a later section), and are therefore restricted to this type of geometry.

$$f_{\mathrm{fund}}^{P} = \frac{\alpha_1}{4h}\sqrt{1 + \left(\frac{h}{l}\right)^2} \qquad (2)$$

$$f_{\mathrm{fund}}^{\mathrm{SV}} = \frac{\beta_1}{4h}\sqrt{1 + \left(\frac{2.9h}{l}\right)^2} \qquad (3)$$

where h is the maximum sediment depth, l the half-width of the sine type I valley, and α_1 and β_1 are the *P*- and *S*-wave velocity, respectively, and h/l is the so-called "shape ratio."

Using the results of the modeling work of Bard and Bouchon (1985), we derived the pattern of spectral amplitudes for the SH-, SV-, and *P*-ground motion across a valley profile; the results are displayed as qualitative sketches in Figure 3 for the two different analysis techniques used. The amplification pattern of higher order modes with nodes in vertical direction ($m > 0$) in the SH case and of higher order PSV modes is more complex and no simple sketches can be given for them.

To describe the horizontal motion due to the resonance phenomena, we define here the horizontal motion parallel to the valley axis as transversal and the horizontal motion perpendicular to it radial.

Microtremors: RSM and H/V Methods

In areas of low seismicity, microtremors are the most suitable instrument to obtain information about the local site conditions and possible site effects. In past years, the measurement of ambient vibrations has been used in a wide range of scientific work (e.g., Celebi *et al.*, 1987; Lermo *et al.*, 1988; Field *et al.*, 1990; Hough *et al.*, 1992; Fäh *et al.*, 1997). Early investigations demonstrated that seismic noise depends on the time of the day (Udwadia and Trifunac, 1973), reflecting more source effects rather than site characteristics. Special analysis techniques have been developed to eliminate these source effects in the spectra of the microtremor signal: the RSM (Ohta, 1978; Kagami, 1982, 1986) and the H/V method (Nakamura, 1989). Both methods have been used successfully in previous studies (e.g., Lachet and Bard, 1994; Lermo and Chávez-García, 1994; Field and Jacob, 1995; Fäh *et al.*, 1997).

The RSM compares the amplitude Fourier spectra of the single components recorded on a soft-soil site with those at a reference station on bedrock (e.g., Field *et al.*, 1990; Yamanaka *et al.*, 1993; Lermo and Chávez-García, 1994). The original method uses signals from long-distance earthquakes under the assumption that source and path effect are identical at the soil and bedrock stations. When using ambient vibrations, this important condition is not necessarily fulfilled. However, long-period microtremors are caused by ocean waves and have long-distance sources when measured in inner continental regions such as Switzerland. They therefore have stable spectra for longer periods of time (Bard, 1998). Field and Jacob (1993) assumed that the noise spectra were white before entering the sediment valley, ensuring that the source and path effects were statistically equal at the two stations during long recording periods.

The H/V method uses spectral ratios of a single station to obtain fundamental resonance frequencies. It has been frequently used in Japan and has become popular in the Western world after its publication by Nakamura (1989). The method is based on the assumption that at any site the

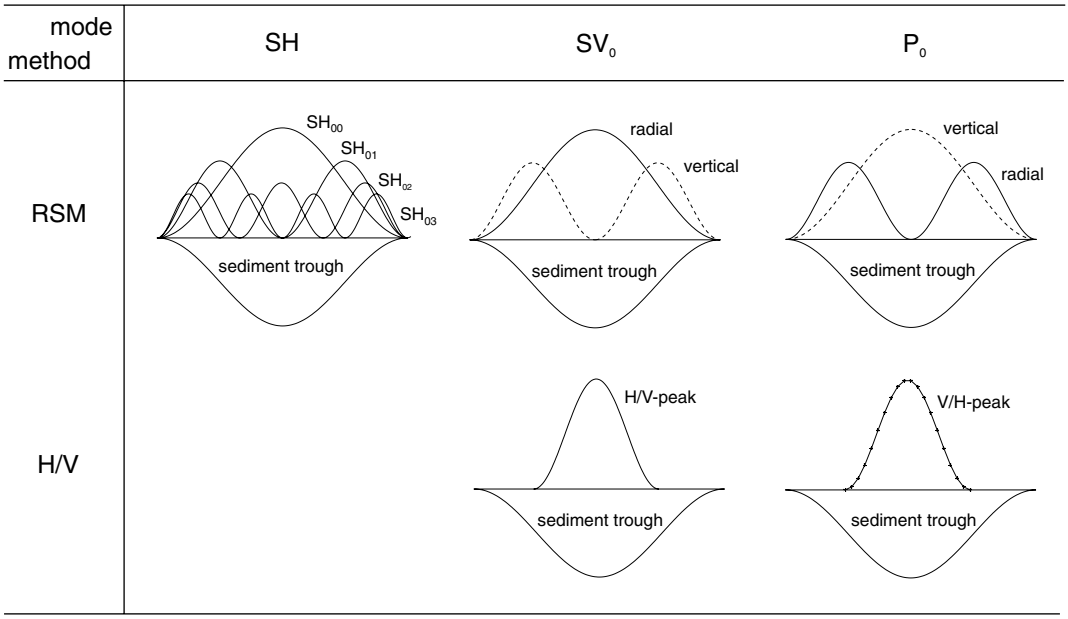

Figure 3. Expected pattern of spectral amplitudes when analyzing spectral ratios obtained with RSM and H/V ratios in a type I sine-shaped valley. In the SH case some higher modes are given (SH_{00}, fundamental; SH_{01}, first higher antisymmetrical; SH_{02}, first higher symmetrical; SH_{03}, second higher antisymmetrical mode); in the PSV case only the expected shape of the fundamental modes are shown.

vertical component of seismic noise is essentially unaffected by site effects, whereas the horizontal components are strongly influenced by the presence of soft soils. The fundamental frequency of resonance can thus be estimated from the ratio of the H/V Fourier spectra. Lachet and Bard (1994) and Dravinski *et al.* (1996) showed that the H/V method can be used to determine the fundamental mode in 1D, 2D, or 3D structures, but that the amplitudes of the H/V peaks cannot be used to predict amplification values of ground motion at the specific site.

Figure 3 illustrates the different resonance modes over a simplified sediment structure giving the expected pattern of spectral ratios calculated with the RSM and the H/V technique. Note that a single narrow peak on the H/V ratio identifies the SV fundamental, whereas the P fundamental can be detected on the inverse V/H ratio.

Numerical Investigations of Synthetic Microtremors for the 2D St. Jakob–Tüllingen Trough

To study the resonance properties of the St. Jakob–Tüllingen syncline, we first approximated the shape of the structure by two sine-type geometries (hereafter named type I and type II valleys). (Note that this nomenclature does not correspond to the type 1 and type 2 definitions used in the Bard and Bouchon 1980a,b pulications.) This allowed us to test our modeling approach by comparing the resonance frequencies found in the synthetic microtremor wave field with the results of the calculated frequencies of resonance using the formulas by Bard and Bouchon (1985). A type I syncline is bounded by two neighboring maxima of a sine curve and corresponds to the sine valley geometry used in Bard and Bouchon (1985). A type II valley extends between two zeros of the sine curve (Fig. 2A). A geological cross section (Gürler *et al.*, 1987; Hauber, 1991) has been used as the basis for the realistic model of the St. Jakob–Tüllingen trough. Figure 2B shows the model as it was used in the computations together with the shape of the approximated sine valleys. The physical parameters of the models were taken mostly from existing studies (Schweizerischer Erdbebendienst [SED], 1997), complemented with sonic-log recordings from deep drillholes in a nearby region (Weber *et al.*, 1986). Where no data for specific rock types were available, parameters were derived from standard compilations (Clark, 1966). The quality factors were estimated.

To calculate the microtremor wave field in the valley, a finite-difference (FD) method for inelastic *SH*- and *PSV*-wave propagation was used (Fäh, 1992). For each model (both sine-type models and the realistic model), a 2D synthetic microtremor wave field was calculated at 44 equally spaced receiver positions along a profile across the syncline. The first receiver was located at a distance of 500 m from the left model boundary of the FD grid. Because we do not know the nature of the microtremors, we generated them on the left side of the model by a small band of randomly spaced point sources radiating random signals (Fig. 2B). With this configuration, source effects are to be expected due to the small source-receiver distance. Synthetic microtremors have a duration of 450 sec. Grid spacing of 10 m was used, with a total model dimension of 1000 $\times$ 300 grid points.

The synthetic microtremors were analyzed using the RSM and the H/V methods. For the RSM analysis, the time signals were split into windows of 80 sec with 50% overlap, and spectral ratios against the reference station signal (station 44) were calculated for each time window and then averaged over the windows. We display the mean RSM spectral ratios for each frequency and station position (Figs. 4A and 5A) to identify consistent peaks across the valley. Spectral ratios at specific resonance frequencies are displayed along profiles (Figs. 4B and 5B) to visualize 2D features in the same way as given in the sketches of Figure 3. The frequency range below 0.2 Hz is not shown because of major source effects. In Figures 4C and 5C we show spectral ratios at the selected receiver positions indicated by a thin black line in part A of the corresponding figure. In these figures the mean value of the spectral ratio of the different time windows is given in a solid black line. The gray shading shows the standard deviation of the mean spectral ratio and therefore indicates the sharpness of the peaks analyzed. We used the width of the standard deviation band (grey shaded area) on the ordinate level of the peak maxima as the measure of uncertainty and display it in the summary table of the corresponding dataset (Table 1).

The synthetic H/V spectral ratios are only computed for the *PSV* case, that is, the ratio of the radial and the vertical component was used. Again the time signals were split into windows of 80 sec with 50% overlap, and the ratios of the Fourier spectra were calculated and averaged. Because of specific problems we had using the H/V method and which will be discussed later, we display only very few results of this analysis. Figures 4D and 5D give series of cross sections at specific frequencies, which are indicated in the figures.

The RSM results of the analysis of the synthetic data for the three models (types I and II sine shape, realistic model) are shown in Table 1. The first column for each model gives the theoretical frequencies estimated using the formulas by Bard and Bouchon (1985). Because the formulas for the *SV*- and *P*-fundamental frequencies are only valid for the type I sine-shaped valley, the resonance frequencies for the other models are estimated based on the assumption that the broader the valley is the lower the resonance frequencies are. The second column gives the frequencies found for the corresponding resonance modes in the modeling data.

Sine Model Type I

The RSM results for the type I sine-shaped model show three clearly excited *SH* modes, the *SV* fundamental as well as a higher *SV* mode (Fig. 4A). We note the strong excitation of the first higher antisymmetrical mode (SH_{01}) at 0.48 ± 0.01 Hz and the weaker excitation of the *SH* fundamental (SH_{00}) at 0.38 ± 0.02 Hz (Fig. 4B). The two resonance modes seem to overlap but can be separated by looking at the cross sections in the corresponding frequency band. We use the "predicted resonance frequency" using the Bard and Bouchon (1985) formulas and the "peak geometry" (Fig. 3) to identify the most dominant peaks and find good agreement between those frequencies. We identify the 0.41 ± 0.02 Hz peak as the *SV* fundamental. The overall geometry on the radial and vertical components shows a good fit to the expected shape of the *SV* fundamental (Fig. 3).

On the radial component in Figure 4A, a weak signal is visible just below the strong 0.41-Hz peak. We investigated our hypothesis that this signal corresponds to a numerical effect by varying the model parameterization and enlarging the initial model size to 1400 × 350 grid points. The peak at 0.41 Hz remained stable in frequency and geometry, whereas the weaker peaks at lower frequencies changed in frequency and shape when we modified the source location, model size, and internal geometry (distance of the trough from the model boundary). We conclude that the weak peak below the strong 0.41 peak can be considered as an artifact of the modeling work and has no physical meaning.

The pattern of spectral amplitudes around 0.9 Hz, the expected resonance frequency for the fundamental P mode, in both radial and vertical components is too complex to allow an estimate of this resonance mode. It is possible that it has not been excited at all.

To discuss the H/V data we display a series of cross sections at constant frequencies in Figure 4D. We show the frequency range between 0.31 and 0.42 Hz in which two distinct maxima can be seen at 0.35 and 0.41/0.42 Hz. The latter would fit to the observation of the SV fundamental in the RSM data but has its most pronounced maximum around station 13 and not over the region of the sedimentary trough (between stations 21 and 38). The main peak at 0.35 Hz lies between these two stations and would therefore better fit to the expectations of a *SV* fundamental in the H/V data but the frequency lies clearly below the 0.41 Hz of the RSM analysis. However, the results of H/V analysis allow no clear detection of the *SV* fundamental. The origin of the many spectral peaks outside the sedimentary trough may indicate a strong influence of the source band to the left of the model. We have reached the limits of H/V method. This approach is unsuitable to detect 2D resonances in microtremor data when source effects dominate the characteristics of the ambient vibration wave field.

Sine Model Type II

In the next step we used a slightly different sine model to approximate the St. Jakob–Tüllingen trough (signals not shown, results in Table 1). The *SH* fundamental is not excited at all, whereas the first higher antisymmetrical *SH* mode (SH_{01}) and the SV_0 mode dominate the microtremor wave field. The broader geometry of the type II valley leads to a general slight decrease of the resonance frequencies in the valley (Table 1). The incidental wave field controls the eigenvibrations of the structure.

St. Jakob–Tüllingen Model

The RSM analysis of the synthetic microtremors for the realistic structural model of the St. Jakob–Tüllingen trough (Fig. 5A) reveals several consistent maxima. Due to the asymmetry of the syncline (Fig. 2B) the right-hand-side boundary of the trough is well defined at station 40, whereas at the left-hand-side boundary the thickness of the sediment cover decreases slowly. Cross sections at specific frequencies of large spectral ratios show the shape of spectral peaks in the syncline (Fig. 5B). A comparison of the frequencies of the peaks of spectral ratios with the expected ones suggests (Table 1) that: the 0.37 ± 0.03 Hz maximum corresponds to the first higher antisymmetrical *SH* mode (SH_{01}); the fundamental mode would have a lower frequency and is therefore not excited; the shape of the pattern of spectral amplitudes at 0.42 ± 0.04 Hz corresponds to the first higher symmetrical mode (SH_{02}); and the pronounced amplification and geometry of the peaks at 0.53 ± 0.02 Hz peak correspond well to the second higher symmetric *SH* mode (SH_{04}).

The results of the RSM on the radial and vertical component show the *SV* fundamental at a frequency of 0.31 ± 0.02 Hz. The P fundamental is not seen, but several higher *SV* modes are identified on the basis of their frequency and their significant amplitudes (between 6 and 12 on the radial component) of their spectral ratios. A certain asymmetry in all curves is obvious, and is explained by the close distance of the source zone and by the structural asymmetry of the syncline.

The H/V results will again be discussed using a series of constant frequency cross sections. The cross sections cover a frequency range between 0.28 and 0.39 Hz. The expected *SV* fundamental has been detected in the RSM data at 0.31 Hz. At this frequency we do detect a very sharp and high spectral peak, but when looking at the cross sections at lower and higher frequencies, we find similar peaks in the frequency range from 0.28 to 0.30 and at 0.32 Hz. At 0.33 Hz a double peak marks the transition to a very sharp spectral peak with slightly lower spectral amplitudes around station 11. Again the *SV* fundamental, which was clearly visible in RSM data, cannot be detected by the H/V method leading to the same conclusions we made when analyzing the sin type I model data: H/V method cannot be used for the detection of 2D resonances in 2D structures in the way presented here.

Numerical Investigations of Synthetic Microtremors for the 2D Rhone Valley near Vetroz

The resonance properties in the Rhone valley near Vetroz were investigated using a realistic cross section in the region based on geological information from a reflection seismic study (Pfiffner *et al.*, 1997) and the work by Frischknecht *et al.* (1998). A slight simplification of the model was applied by introducing horizontal layers in the sedimentary trough. FD-model dimensions are 890 × 300 grid points with grid spacing of 10 m. Again we placed the first receiver at a distance of 500 m from the left model boundary where the random sources were located. We calculated the resulting synthetic signal of 240 sec duration for 38 different receiver positions, each receiver spaced 100 m apart from its neighbors. We used station 1 as reference station. On the basis of the experiences of the previous analysis, the synthetic signals were only analyzed using the RSM method. The results are displayed in Figure 6A–C, and Table 2 summarizes the resonance frequencies and uncertainties. The results from the *SH* case in Figure 6A and B show clearly the first four *SH* modes ($SH_{00–03}$) at 0.29 ± 0.02, 0.38 ± 0.01, 0.47 ± 0.01, and 0.55 ± 0.02 Hz, respectively. The *SV* fundamental at 0.34 ± 0.01 Hz as well as a higher *SV* mode at 0.57 ± 0.02 Hz can be seen on the radial and vertical component of the corresponding figures. The results are much more clear than in the St. Jakob–Tüllingen model. The reason for this must be the higher impedance contrast between the sediment fill

Table 1

Predicted (Pred.) Resonance Frequencies Versus the Ones Derived Using RSM on Synthetic Microtremor Data for Two Sine-Type (I and II) and the St. Jakob–Tüllingen Model (SV_X corresponds to the Higher SV Mode)

	Type I Model		Type II Model		St. Jakob–Tüllingen Model	
Mode	Pred.	Modeled (RSM)	Pred.	Modeled (RSM)	Pred.	Modeled (RSM)
SH_{00}	0.35	0.38 ± 0.02	0.32		0.31	
SH_{01}	0.48	0.48 ± 0.01	0.40	0.43 ± 0.01	0.34	0.37 ± 0.03
SH_{02}	0.63		0.51	0.51 ± 0.02	0.41	0.42 ± 0.04
SH_{03}	0.81	0.84 ± 0.02	0.63	0.63 ± 0.01	0.48	
SH_{04}	0.99		0.76	0.72 ± 0.02	0.56	0.53 ± 0.02
SV_0	0.40	0.41 ± 0.02	~0.3–0.4	0.35 ± 0.01	~0.3	0.31 ± 0.02
SV_X		0.55 ± 0.02		0.51 ± 0.01		0.46 ± 0.02
SV_X				0.57 ± 0.03		0.51 ± 0.02
SV_X						0.66 ± 0.02
P_0	0.91		0.7–0.8		~0.7	

(a)

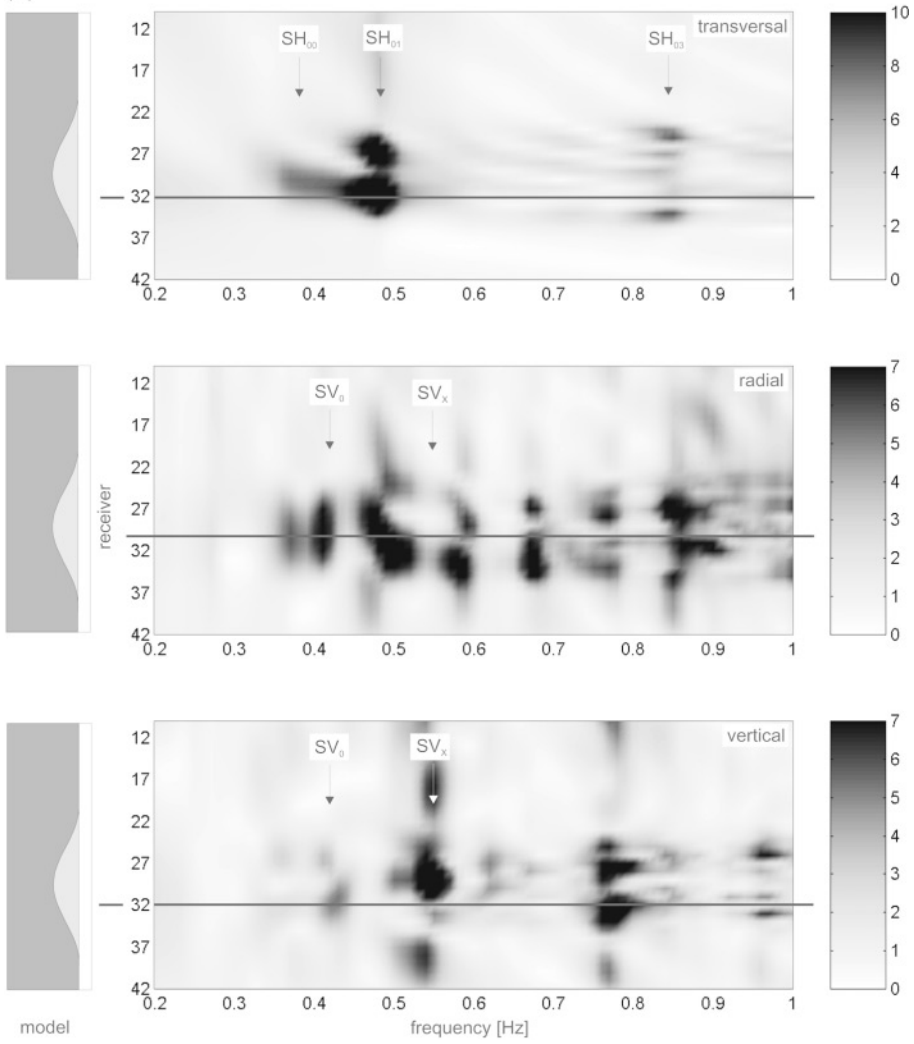
transversal
radial
vertical
receiver
model
frequency [Hz]

(b)

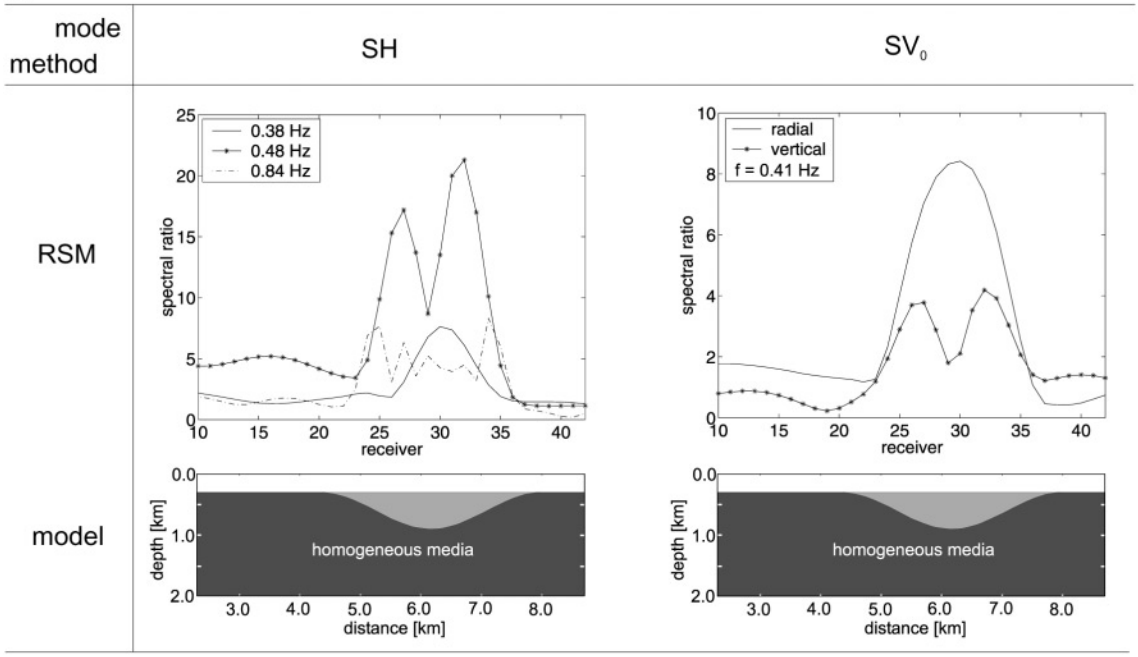
mode
method
SH
SV0
RSM
model
0.38 Hz
0.48 Hz
0.84 Hz
radial
vertical
f = 0.41 Hz
spectral ratio
receiver
depth [km]
homogeneous media
distance [km]

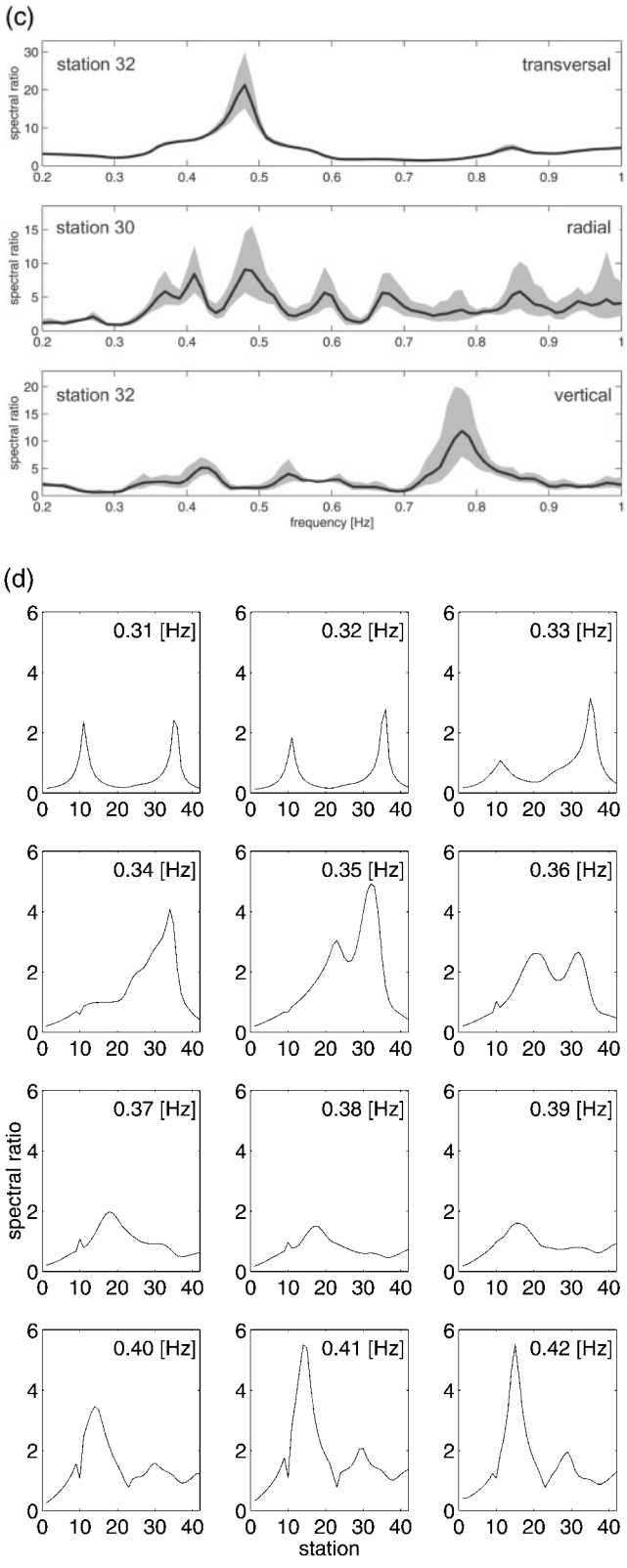

Figure 4. Numerical modeling for the sine-shaped type I model. (a) Results of RSM. The three blocks display the RSM data for the three components of movement: transversal, radial, and vertical. Each block contains the spectral ratios in the frequency range between 0.2 and 1 Hz (x axis) of all receivers stringed along the y axis. The sketch of the model to the left of each data block can be used to find the receiver positions with respect to the position in the sedimentary basin. Dark spots in the spectral ratio data indicate high values. Arrows point to and label specific modes of resonance discussed in the text and partly shown in Figure 4B. The horizontal black lines give the position of the single receiver data shown in Figure 4C. The frequencies and uncertainties of the corresponding resonance modes can be found in Table 1. (b) Constant frequency cross sections through RSM spectral ratio data. SH case, SH_{00} at 0.38 $\pm$ 0.02 Hz, SH_{01} at 0.48 $\pm$ 0.01 Hz, and SH_{03} at 0.84 $\pm$ 0.02 Hz. PSV case, RSM ratios indicate the SV-fundamental mode at 0.41 $\pm$ 0.02 Hz. For comparison, the model is included with an approximate match to the figures above in each column. (c) Single receiver spectral ratios (RSM) showing mean spectral ratios (solid black line) and mean plus-and-minus one standard deviation in gray patches. As a measure of uncertainty, the width of the gray area on the ordinate level of the maximum mean peak was used. (d) Constant frequency cross sections trough H/V spectral ratios in the frequency range between 0.31 and 0.42 Hz. Two peaks at 0.35 and 0.41/0.42 Hz show local maxima but cannot be associated with the results of the RSM analysis.

(a)

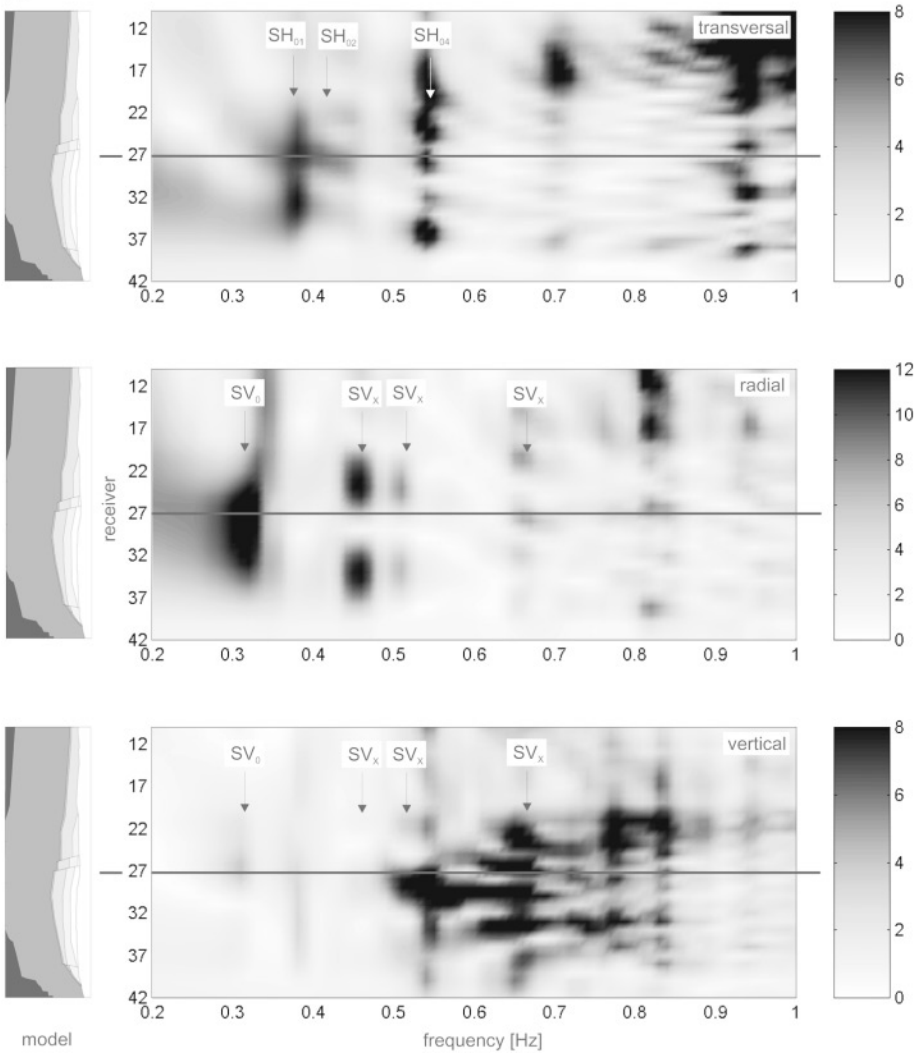
transversal
radial
vertical
receiver
model
frequency [Hz]

(b)

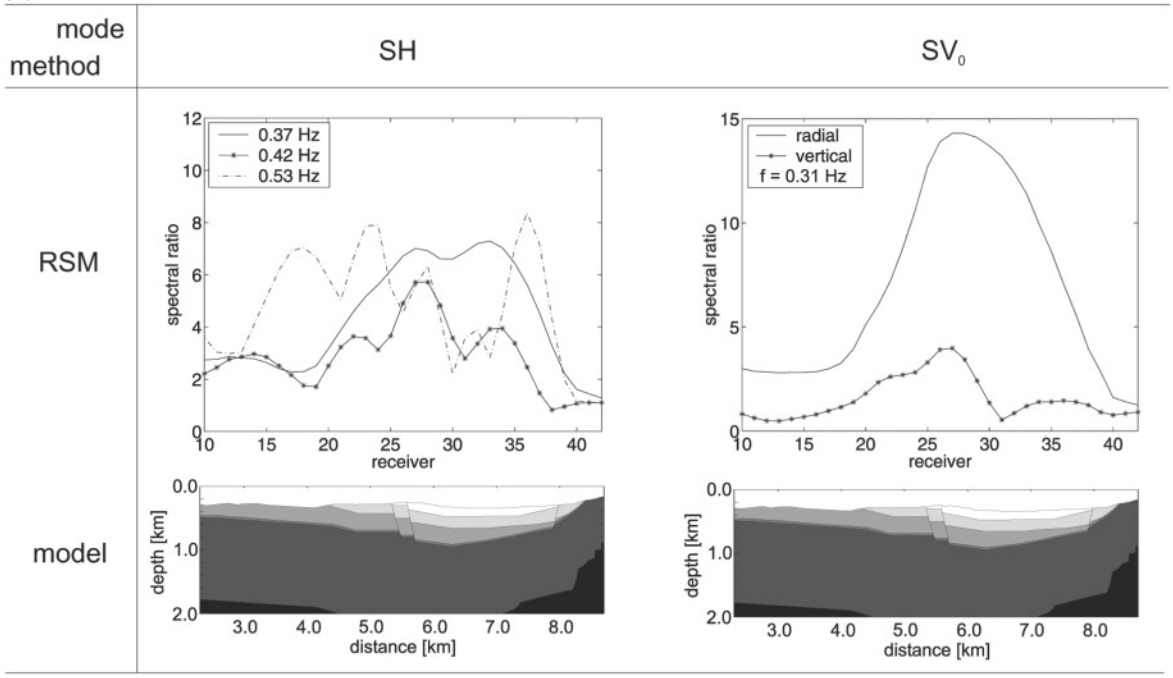
mode
method
SH
SV0
RSM
model
0.37 Hz
0.42 Hz
0.53 Hz
radial
vertical
f = 0.31 Hz
spectral ratio
receiver
depth [km]
distance [km]

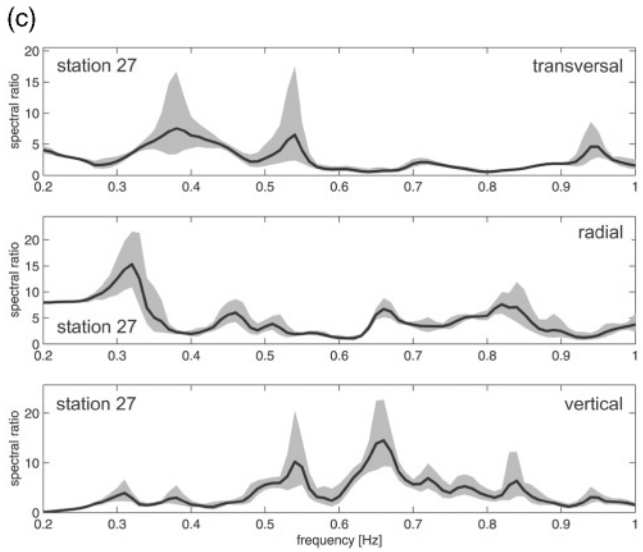

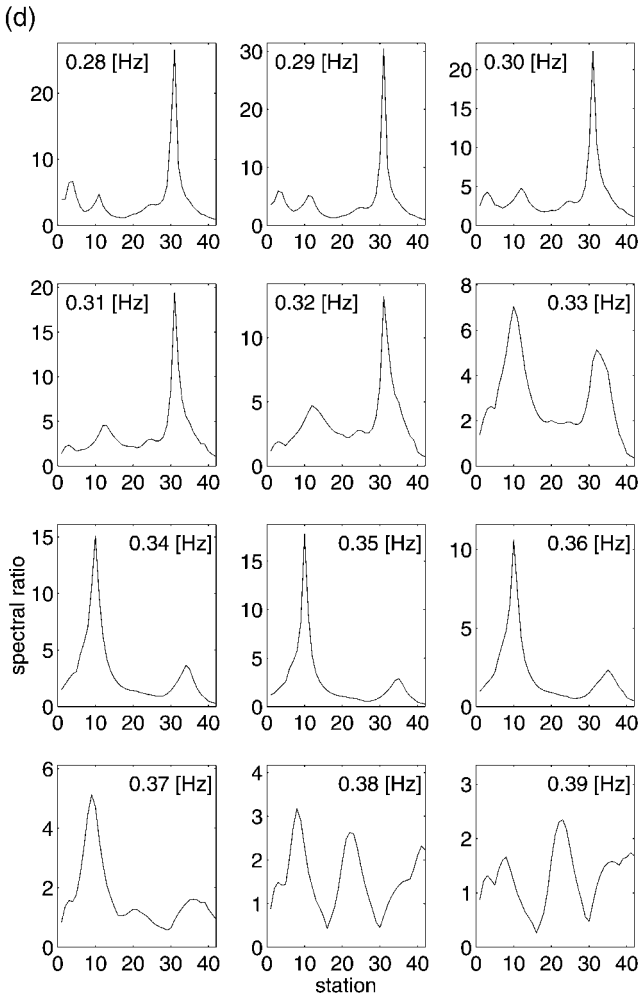

Figure 5. (a–c) The same as Figure 4 except we used the St. Jakob–Tüllingen model. The values of the corresponding resonance modes are in Table 1. (d) Constant frequency cross sections trough H/V spectral ratios in the frequency range between 0.28 and 0.39 Hz. Two sharp maxima at station 31 at lower frequencies and at station 11 at higher frequencies dominate the spectra allowing no identification of the SV fundamental.

(a)

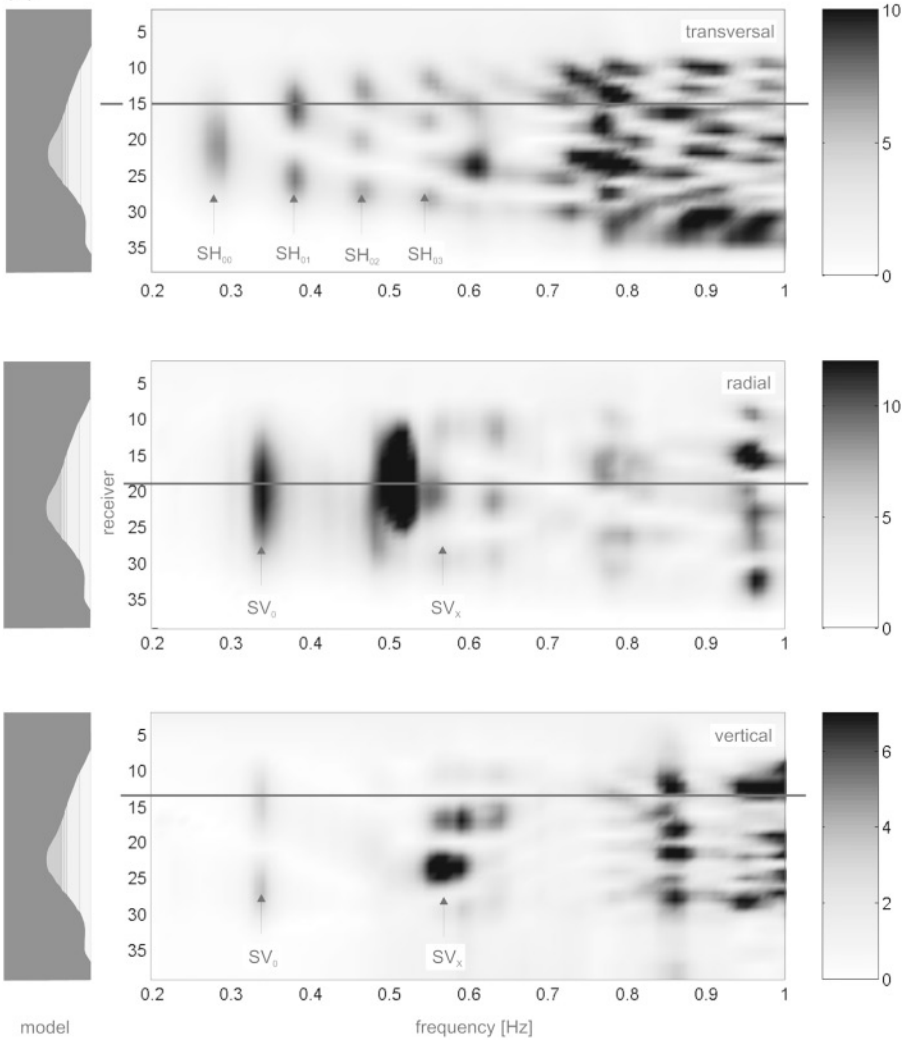
transversal
radial
vertical
receiver
SH00
SH01
SH02
SH03
SV0
SVx
model
frequency [Hz]

(b)

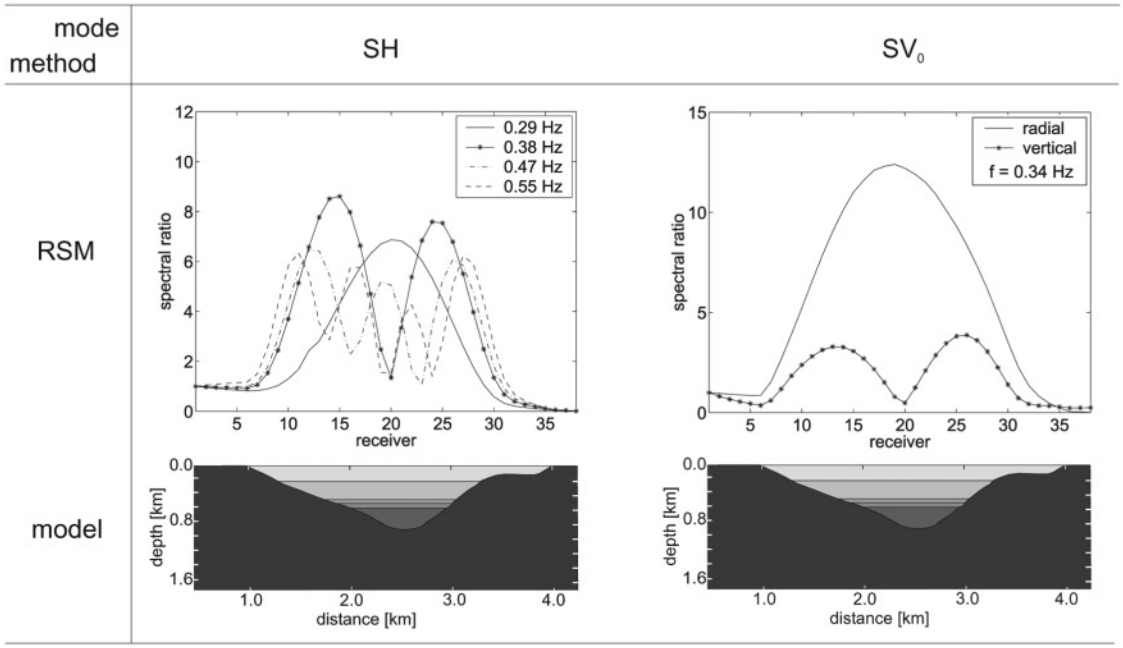
mode
method
SH
SV0
RSM
model
0.29 Hz
0.38 Hz
0.47 Hz
0.55 Hz
radial
vertical
f = 0.34 Hz
spectral ratio
receiver
depth [km]
distance [km]

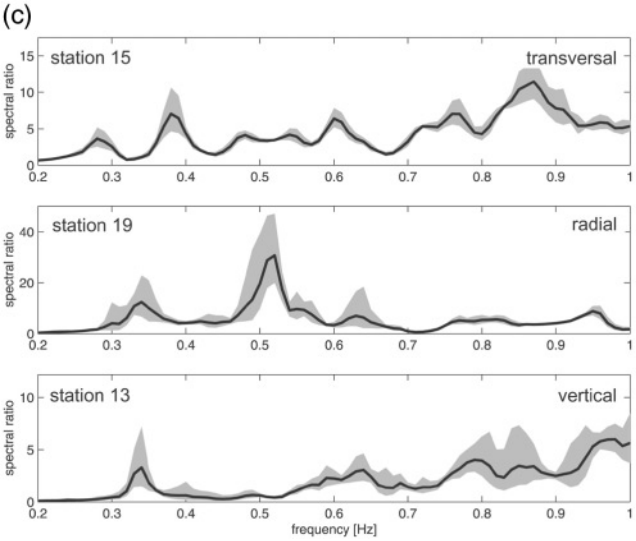

Figure 6. (a–c) The same as Figure 4 except we used the Vetroz model. The values of the corresponding resonance modes are in Table 2. No H/V ratios are shown.

and the valleys bedrock and a clearer geometrical structure with less asymmetries than in the St. Jakob–Tüllingen case.

Analysis of Recorded Microtremors

St. Jakob–Tüllingen Trough

To compare the seismic behavior of the St. Jakob–Tüllingen trough with the synthetic results, simultaneous measurements of microtremors were performed along the profile perpendicular to the strike of the fault axis given in Figure 1A as profile line and as geological cross section and model sketch in Figure 2B. We used five three-component seismometers with a natural period of 5 sec in the measurement campaign.

The reference signal, necessary in the RSM analysis, was recorded outside the Rhinegraben on a presumed bedrock site (station R in Figs. 1A and 2B). The remaining four receivers A, B, C, and D in Figs. 1A and 2B) were placed on top of the sediments filling the St. Jakob–Tüllingen syncline, covering only about half of the width of the trough. This was done to get the minimum data density necessary to define the geometry of the expected resonance modes and to have a comparable microtremor signal throughout the whole measurement area.

To get results comparable with the modeling presented previously, we oriented the receivers having one horizontal component parallel to the measurement line A to R (this corresponds to the "radial" component defined previously) and the other parallel to the strike of the fault axis of the St. Jakob–Tüllingen trough (the "transversal" component). It is obvious that the separation of the two measured horizontal components, and therefore the separation between the SH and SV and P modes, cannot be as clear as in the modeling work, where the two synthetic horizontal components were generated using separate calculation codes.

We measured during November and therefore expect the microtremors in our study area to be mostly generated by winter storms in the Atlantic Ocean in a general westerly azimuth. This westerly azimuth corresponds to the source band concentrated to the left of the structure in our modeling approach. The influence of very local noise sources in this low-frequency range is assumed to be of minor importance, and the measurement duration of half an hour should provide enough data to average the influence of such local sources.

The measurements were analyzed with H/V and RSM data. The H/V results only show one significant, consistent peak at 0.39 Hz (results not shown). This peak must have the same origin as the ones noticed in the previously mentioned measurement campaign by Fäh *et al.* (1997) where many measurements of H/V ratios have revealed a uniform resonance frequency at about 0.4 Hz in the St. Jakob–Tüllingen trough (Fig. 1A).

The RSM spectra for all receiver positions are shown in Figure 7. The mean spectra were only calculated with those microtremor signal parts showing no unusual transients with very high amplitudes. It is noted that the amplitudes of the spectral peaks are very low. With few exceptions they are lower than a factor of 2, which is usually considered as minimum uncertainty when dealing with earthquake data (e.g., King and Tucker, 1984). The range of uncertainty (band of standard deviation) here is very broad, too, and the single peaks are not very distinguishable from each other. We therefore only tentatively marked peaks that are consistent throughout the valley. We associated them to peaks that we have found in the modeling section making the assumption that their consistency throughout the valley is due to a 2D effect visible in the data. Table 3 shows the result of this approach. The frequencies compare fairly well between the model and the measurement results. We found four SH modes as well as three higher SV modes in the data. Most of the peaks in the measurement data are within the error band of the synthetic data. Only the peaks at 0.41 and 0.58 Hz could not be matched to the model results within the range of uncertainty, and no sign of the *SV* fundamental could be found in the measurement data. It possibly has not

Table 2
Predicted Resonance Frequencies Versus the Ones Derived Using RSM on Synthetic Microtremor Data Calculated for the Vetroz Site

Mode	Predicted	Modeled
SH_{00}	0.30	0.29 ± 0.02
SH_{01}	0.36	0.38 ± 0.01
SH_{02}	0.45	0.47 ± 0.01
SH_{03}	0.56	0.55 ± 0.02
SV_0		0.34 ± 0.01
SV_X		0.57 ± 0.02

been excited at all. Because of the low receiver density, we could not interpret the pattern of spectral amplitudes in cross sections to identify the type of resonance mode. When we again looked for an explanation of the stable 0.4-Hz resonance frequency values found in the study by Fäh *et al.* (1997), no single mode of resonance could explain the phenomenon. Both, the SH_{01} at 0.39 Hz and the SV_X mode at 0.41 Hz, or a mixture of both can be the reason for the observation. It must be clearly noted that the results just presented cannot be seen as a proof for the existence of 2D resonances in the specific sedimentary structure. The peaks in the RSM data are not well developed. Despite all this, we present these data together with a tentative approach to analyze the data, and we do this for two reasons: we first want the reader to be aware of the various problems arising in such measurement campaigns. Possible reasons for the failure of this specific attempt are a bad reference site, 3D effects which cannot be caught by the 2D approach made in the modeling part, or even local low-frequency sources of noise which disturb the measurements. Second, we wanted to show a difficult case in contrast to the data of the second test site, which looks more promising.

Rhone Valley near Vetroz

For the measurement campaign in the Rhone valley we used a slightly different approach than in the Basel area. Instead of doing simultaneous measurements with our limited number of receivers, we measured microtremor signals at 15 different positions in the valley, one point after another leading to a measurement point density about half that used in the modeling work. Measurement duration was 15 min per point. The field crew consisting of two persons needed one day for the whole measurement campaign. The reference station was situated on a well-defined bedrock site and measured at the same time as all 15 receivers in the valley. A sketch of the measurement positions is given in Figure 2C. The data were analyzed with the RSM only because of the better results obtained in the previous analysis. As in the analysis of the measurement data of the Basel site, only those parts of the signal were used that did not show unusual amplitudes caused most probably by nearby sources. Figure 8 shows a selected number of RSM results taken from different receivers. Vertical black lines mark the most dominant peaks, which can be related to our modeling results. This time the amplitudes of the spectral peaks are high. The different peaks can be distinguished from each other and a measure of uncertainty can be read from the standard deviation. Table 4 summarizes the results. The correspondence between the peaks of the modeling results is within the uncertainty. We find the SH_{00} mode at 0.32 $\pm$ 0.03 Hz and the *SV* fundamental at 0.35 $\pm$ 0.03 Hz. Higher modes seem to be visible in certain spectral ratios, such as in MP 9 on the transverse component, for example, but they cannot be consistently identified in all ratios. Again, cross sections at constant frequency could not be made, this time because the measurements have not been performed simultaneously.

Table 3
Results of a Tentative Comparison of Consistent Peaks of Resonance in the Measurement Data Analyzed with RSM with the Synthetic Ones of the St. Jakob–Tüllingen Site

Mode	Measurement RSM (Hz)	Model RSM (Hz)
SH_{01}	0.39	0.37 $\pm$ 0.03
SH_{02}	0.44	0.42 $\pm$ 0.04
SH_{03}	0.48	0.46 $\pm$ 0.02
SH_{04}	0.58	0.53 $\pm$ 0.02
SV_X	0.41	0.46 $\pm$ 0.02
SV_X	0.51	0.51 $\pm$ 0.02
SV_X	0.64	0.66 $\pm$ 0.02

Table 4
Comparison of the Measurement and the Modeling Results Analyzed with RSM for the Rhone Valley near Vetroz

Mode	Measurement RSM (Hz)	Model RSM (Hz)
SH_{01}	0.32 $\pm$ 0.03	0.29 $\pm$ 0.02
SV_0	0.35 $\pm$ 0.03	0.34 $\pm$ 0.01

Therefore, we have to rely on the synthetic results to identify the type of 2D resonance. Future studies with simultaneous measurements must show if the proposed approach used for the analysis of the modeling data (frequency prediction and interpretation of the pattern of spectral amplitudes) can in fact be applied to measured data.

Conclusions

Observation of very low H/V resonance frequencies in a 2D structure near Basel spurred our investigation about the possibilities to identify 2D resonances in a microtremor wave field. We investigated the nature of the microtremor wave field at two different sites, the St. Jakob–Tüllingen trough near Basel and the Rhone valley near Vetroz. We used one analytical and two formulas obtained from numerical computations by Bard and Bouchon (1985) to estimate resonance frequencies in simplified 2D structures, and applied FD modeling to generate a synthetic microtremor wave field in simplified as well as realistic 2D structures. We analyzed profiles of synthetic microtremors with two different methods, RSM and H/V, to identify the type of resonance modes. We successfully used the RSM technique to identify resonance modes in all our synthetic data. The H/V method revealed no nonunique results and could therefore not be used to detect 2D resonances. The values of the predicted resonance frequencies (using the formulas by Bard and Bouchon [1985]) and the ones identified in the synthetic microtremor wave field by our analysis technique corresponded very well within the range of uncertainty. After the modeling part we performed microtremor measurements in the two areas of interest. The measurement data were analyzed mainly using the RSM.

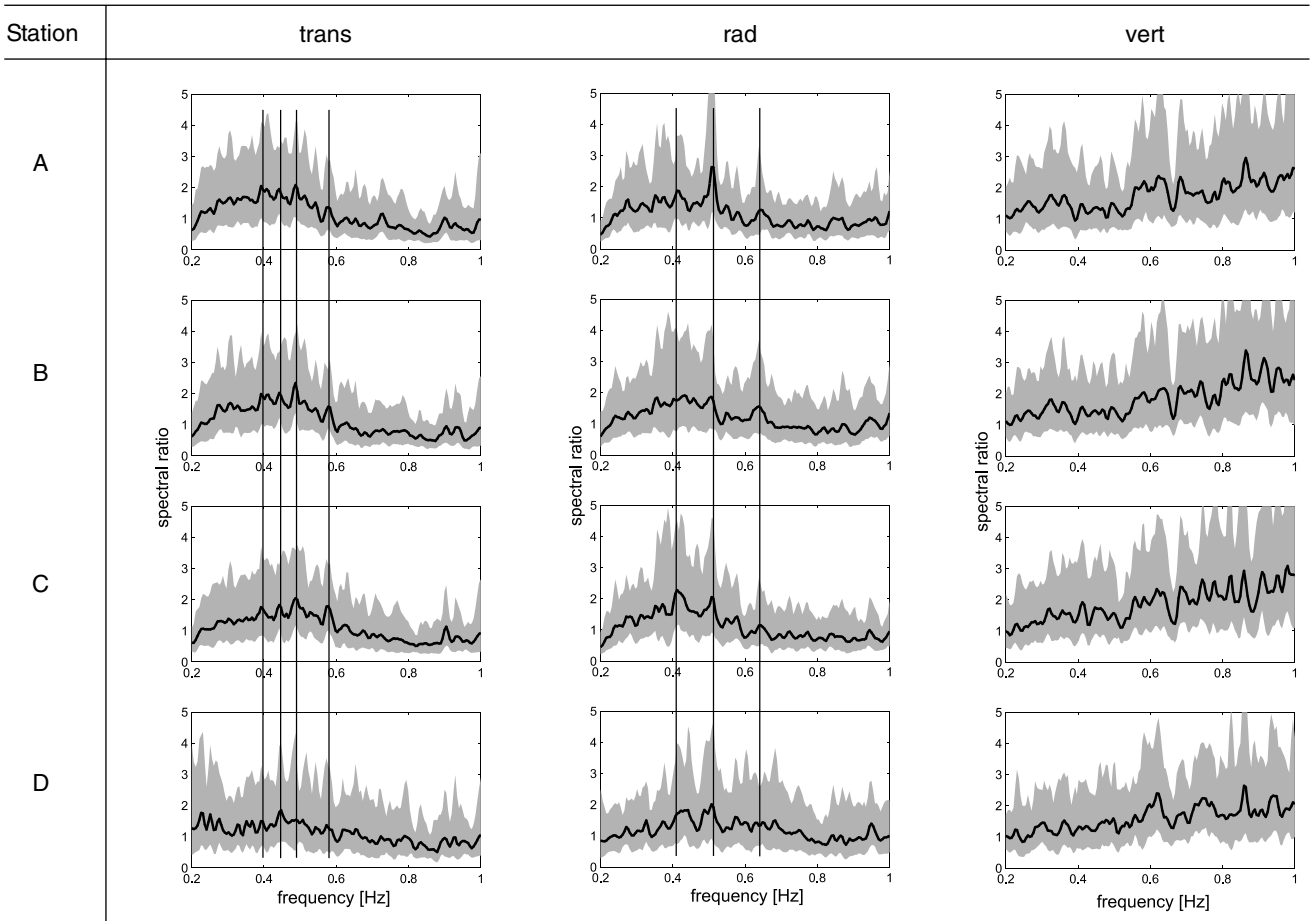

Figure 7. RSM results of the measurements in the St. Jakob–Tüllingen trough for all three components of movement (transversal [trans], radial [rad], and vertical [vert]) in columns and all receivers (A–D) in corresponding lines. The thick black line gives the mean spectral ratio, the gray patch shows the range of plus-and-minus one standard deviation. Vertical lines indicate peaks throughout the different measurement stations that can be tentatively linked to the modeling results. On the transversal component, peaks at 0.39, 0.44, 0.48, and 0.58 Hz were linked to the modeling results indicating modes of resonance SH_{01}, SH_{02}, SH_{03}, and SH_{04}, respectively. On the radial component, peaks at 0.41, 0.51, and 0.64 Hz were correlated to higher SV modes (SV_X). For a discussion on the significance of these results, please refer to the text.

A bad reference station most probably biased the results of the St. Jakob–Tüllingen measurements. As a consequence the spectral peaks had very low amplitudes and could not be distinguished very well from each other. Despite this we could find several consistent peaks in the RSM spectral ratios at the different receivers that could be tentatively correlated to the results of the modeling part. The origin of the constant resonance frequency around 0.4 Hz detected in a previous study in the region could not be associated with a single resonance mode. Possible modes are the SH_{01} mode at 0.39 Hz and a higher *SV* mode at 0.41 Hz.

At the Vetroz site we found much higher spectral amplitudes with peaks that could be distinguished from each other. A match between the synthetic and the measurement results was obtained. We found the SH_{00} mode at 0.32 $\pm$ 0.03 Hz and the *SV* fundamental at 0.35 $\pm$ 0.03 Hz. Future measurement campaigns with high receiver density and simultaneous measurements are needed to investigate the geometry of these two resonance modes in more detail. In addition, they will have to prove if the proposed approach to interpret the pattern of spectral amplifications of RSM data in a profile over a 2D structure can be used to identify the type of 2D resonance mode in measured data.

Acknowledgments

We thank the field crew including Eva Spühler-Lanz, Francesca Bay, Thomas Hottinger, and Daniel Roten for their effort in the cold November. We thank S. Hough, F. Chávez-García, and an anonymous reviewer for their valuable comments, which helped to substantially improve the manuscript.

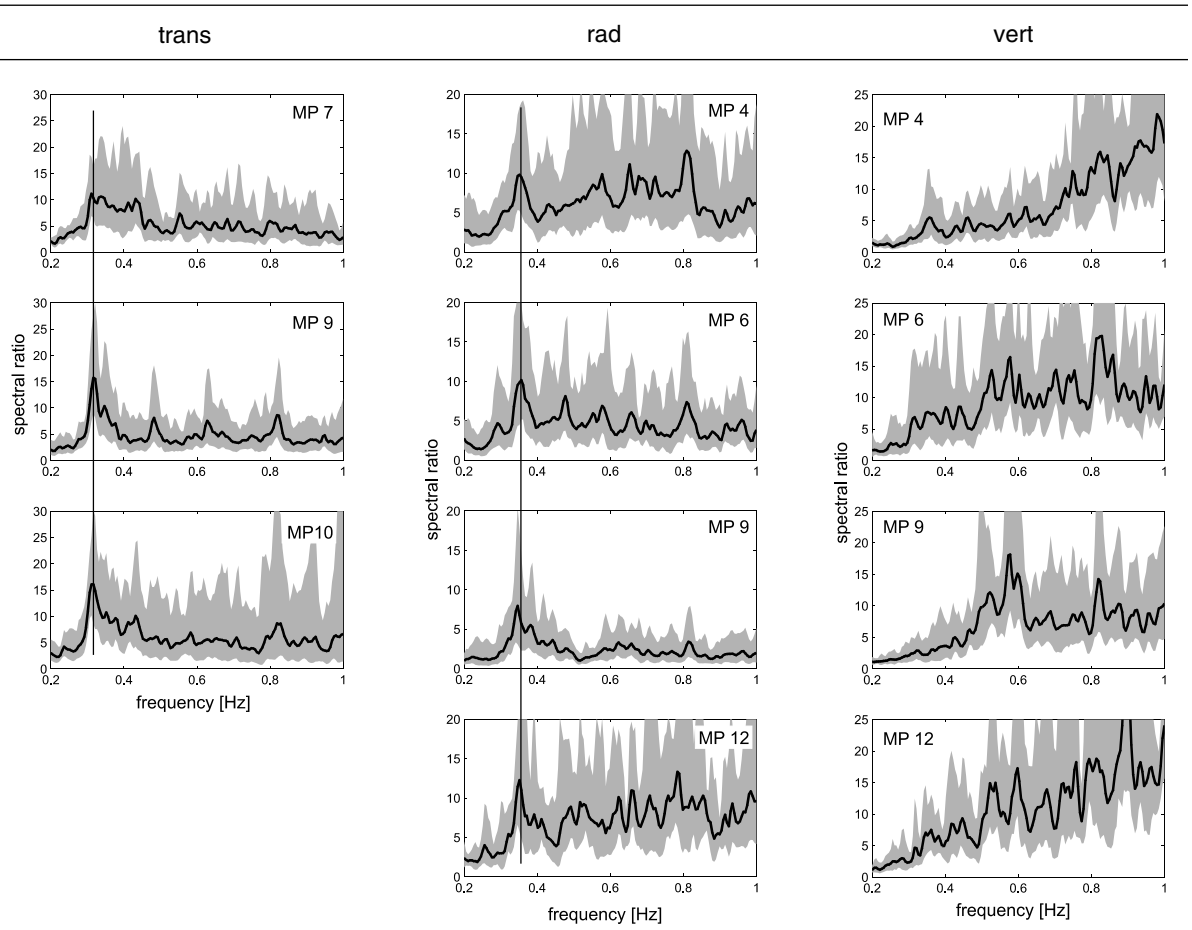

Figure 8. RSM results of the Vetroz measurements for all three components of movement (transversal [trans], radial [rad], and vertical [vert]) in columns and a selection of single receivers (number of receiver in the MP label corresponds to the station numbers of the stations given in Figure 2C). The thick black line gives the mean spectral ratio; the gray patch shows the range of plus-and-minus one standard deviation. Vertical lines indicate resonance peaks, which can be linked to the modeling results. SH_{00} at 0.32 ± 0.03 Hz on the transversal component and the SV fundamental at 0.35 ± 0.03 Hz on the radial component correspond well to these data.

References

Bard, P.-Y. (1998). Microtremor measurements: a tool for site effect estimation?, in *Second International Symposium on the Effects of Surface Geology on Seismic Motion—ESG98*, Yokohama, Japan, 1–3 December 1998.

Bard, P.-Y., and M. Bouchon (1980a). The seismic response of sediment-filled valleys. Part I. The case of incident *SH* waves, *Bull. Seism. Soc. Am.* **70,** 1263–1286.

Bard, P.-Y., and M. Bouchon (1980b). The seismic response of sediment-filled valleys. Part II. The case of incident *P* and *SV* waves, *Bull. Seism. Soc. Am.* **70,** 1921–1941.

Bard, P.-Y., and M. Bouchon (1985). The two-dimensional resonance of sediment-filled valleys, *Bull. Seism. Soc. Am.* **75,** 519–541.

Celebi, M., C. Dietel, J. Prince, M. Onate, and G. Chavez (1987). Site amplification in Mexico City (determined from 19 September 1985 strong-motion records and from recordings of weak motions), in *Ground Motion and Engineering Seismology*, A. S. Cakmak (Editor), Elsevier, Amsterdam, 141–152.

Clark, S. P. (Editor) (1966). *Handbook of Physical Constants*, Revised Edition, *Geol. Soc. Am.* Memoir, Vol. 97, 196–218.

Dravinski, M., G. Ding, and K.-L. Wen (1996). Analysis of spectral ratios for estimating ground motion in deep basins, *Bull. Seism. Soc. Am.* **86,** 646–654.

Fäh, D. (1992). A hybrid technique for the estimation of strong ground motion in sedimentary basins, Diss. ETH Nr. 9767.

Fäh, D., E. Rüttener, T. Noack, and P. Kruspan (1997). Microzonation of the City of Basel, *J. Seism.* **1,** 87–102.

Field, E. H., and K. H. Jacob (1993). The theoretical response of sedimentary layers to ambient seismic noise, *Geophys. Res. Lett.* **20,** 2925–2928.

Field, E. H., and K. H. Jacob (1995). A comparison and test of various site-response estimation techniques, including three that are not reference-site dependent, *Bull. Seism. Soc. Am.* **85,** 1127–1143.

Field, E. H., S. E. Hough, and K. H. Jacob (1990). Using microtremors to assess potential earthquake site response: a case study in flushing meadows, New York City, *Bull. Seism. Soc. Am.* **80,** 1456–1480.

Frischknecht, C., M. Gonzenbach, Ph. Rosset, and J.-J. Wagner (1998).

Estimation of site effects in an alpine valley. A comparison between ground ambient noise response and 2D modelling, in *11th European Conference on Earthquake Engineering*, CNIT, Paris, 6–11 September, Balkema, Rotterdam.

Gürler, B., L. Hauber, and M. Schwander (1987). Die Geologie der Umgebung von Basel mit Hinweisen über die Nutzungsmöglichkeiten der Erdwärme, Beiträge zur geologischen Karte der Schweiz, Leiferung 160 (Neue Folge), Landeshydrologie und geologie und Schweizerische Geologische Kommission (Editors).

Hauber, L. (1991). Ergebnisse der Geothermiebohrungen Riehen 1 und Riehen 2 sowie Reinach 2 im Südosten des Rheingrabens, Geologisches Jahrbuch **E48,** 167–184.

Hauber, L. (1993). Der südliche Rheingraben und seine geothermische Situation, *Bull. Ver. Schweiz. Petroleum-Geol. Ing.* **60,** 53–69.

Hough, S. E., L. Seeber, A. Rovelli, L. Malagnini, A. DeCesare, G. Selveggi, and A. Lerner-Lam (1992). Ambient noise and weak-motion excitation of sediment resonances: results from the tiber valley, Italy, *Bull. Seism. Soc. Am.* **82,** 1186–1205.

Kagami, H., C. M. Duke, G. C. Liang, and Y. Ohta (1982). Observation of 1- to 5-second microtremors and their application to earthquake engineering. Part II. Evaluation of site effect upon seismic wave amplification due to extremely deep soil deposits, *Bull. Seism. Soc. Am.* **72,** 987–998.

Kagami, H., S. Okada, K. Shiono, M. Oner, M. Dravinski, and A. K. Mal (1986). Observation of 1- to 5-second microtremors and their application to earthquake engineering. Part III. A two-dimensional study of site effects in the San Fernando Valley, *Bull. Seism. Soc. Am.* **76,** 1801–1812.

King, J. L., and B. E. Tucker (1984). Observed variations of earthquake motion across a sediment-filled valley, *Bull. Seism. Soc. Am.* **74,** 137–151.

Lachet, C., and P.-Y. Bard (1994). Numerical and theoretical investigations on the possibilities and limitations of Nakamura's technique, *J. Phys. Earth* **42,** 377–397.

Lermo, J., and F. J. Chávez-García (1994). Are microtremors useful in site response evaluation?, *Bull. Seism. Soc. Am.* **84,** 1350–1364.

Lermo, J., M. Rodríguez, and S. K. Singh (1988). The Mexico earthquake of September 19, 1985–natural period of sites in the Valley of Mexico from microtremor measurements and strong motion data, *Earthquake Spectra* **4,** 805–814.

Nakamura, Y. (1989). A method for dynamic characteristics estimation of subsurface using microtremor on the ground surface, *QR RTRI* **30,** 25–33.

Ohta, Y., H. Kagami, N. Goto, and K. Kudo (1978). Observation of 1- to 5-second microtremors and their application to earthquake engineering. Part I: Comparison with long-period accelerations at the Tokachi-Oki earthquake of 1968, *Bull. Seism. Soc. Am.* **68,** 767–779.

Pfiffner, O. A., P. Lehner, P. Heizmann, S. Mueller, and A. Steck (Editors) (1997). *Deep Structure of the Swiss Alps–Results of NRP 20*, Birkhäuser, Basel.

Schweizerischer Erdbebendienst (SED) Geol.–Paleont. Inst. Uni Basel (1997). Erdbebenmikrozonierung für den Kanton Basel-Stadt.

Udwadia, F. E., and M. D. Trifunac (1973). Comparison of earthquake and microtremor ground motions in El Centro, California, *Bull. Seism. Soc. Am.* **63,** 1227–1253.

Weber, H. P., G. Sattel, and C. Sprecher (1986). Sondierbohrungen Weiach, Riniken, Schafisheim, Kaisten, Leuggern–Geophysikalische Daten NTB 85-50, Nagra Technical Reports, Nagra, Wettingen.

Yamanaka, H., M. Dravinski, and H. Kagami (1993). Continuous measurements of microtremors on sediments and basement in Los Angeles, California, *Bull. Seism. Soc. Am.* **83,** 1595–1609.

Institute of Geophysics
ETH Hoenggerberg
CH-8093 Zuerich, Switzerland

Manuscript received 12 October 2000.